Measurement of miniband parameters of a doped superlattice by photoluminescence in high magnetic fields

INSTITUTE OF PHYSICS PUBLISHING JOURNAL OF PHYSICS D: APPLIED PHYSICS

J. Phys. D: Appl. Phys. **37** (2004) 2949–2953 PII: S0022-3727(04)79012-9

Measurement of miniband parameters of a doped superlattice by photoluminescence in high magnetic fields

R F Oliveira[1], **A B Henriques**[1], **T E Lamas**[1], **A A Quivy**[1] **and E Abramof**[2]

[1] Instituto de Física, Universidade de São Paulo, Caixa Postal 66318, 05315-970 São Paulo, Brazil

[2] LAS-INPE, Av. dos Astronautas, 1758-Jd. Granja, 12227-010, São José dos Campos, Brazil

Received 12 April 2004, in final form 30 July 2004
Published 8 October 2004
Online at stacks.iop.org/JPhysD/37/2949
doi:10.1088/0022-3727/37/21/002

Abstract

We have studied a 50/50 Å superlattice of GaAs/$Al_{0.21}Ga_{0.79}As$ composition, modulation-doped with Si, to produce $n = 1.4 \times 10^{12}\,cm^{-2}$ electrons per superlattice period. The modulation-doping was tailored to avoid the formation of Tamm states, and photoluminescence (PL) due to interband transitions from extended superlattice states was detected. By studying the effects of a quantizing magnetic field on the superlattice PL, the miniband energy width, the reduced effective mass of the electron–hole pair, and the band gap renormalization could be deduced.

1. Introduction

The direct measurement of characteristic parameters of low-dimensional semiconductor systems from their optical spectra requires an experimental technique sensitive enough to detect the singularities in the electronic density of states [1–4]. In superlattices, optical detection of the van Hove singularities associated with electronic minibands has been accomplished by measuring the absorption spectrum due to intraband transitions in the far infrared wavelength range [1]. Interband optical methods, however, could not be used successfully to provide a direct measurement of the miniband width, due to the formation of saddle point excitons at the edges of the van Hove singularities [2], with a binding energy which is larger for the M_1 exciton than for the M_0 exciton, due to a negative electronic effective mass along the growth direction in the former case [3]. In heavily doped superlattices, exciton formation is suppressed, due to Coulomb screening and phase-space filling. With sufficient doping, the Fermi level will lie above the energy at the top of the electronic miniband, and luminescence from miniband states below the Fermi level should be observed. One drawback, however, is that often the photoluminescence (PL) of doped superlattices is completely dominated by transitions between localized Tamm states, precluding the detection of interband transitions associated with extended miniband states [4]. When the doping atoms are located in the inner barrier layers of the superlattice, the spatial separation between the electronic charge and the ionized donors gives rise to a strong bending of the band-edges at the boundaries of the superlattice, which causes a shift of the outer wells from resonance with the inner ones, and Tamm states are formed (for a survey on Tamm states in superlattices see [5]).

If the modulation-doping profile is tailored in order to avoid the formation of Tamm states, then it should be possible to detect the miniband singularities by using interband PL spectroscopy. By solving the Schrödinger and Poisson equations, we found that the formation of Tamm states could be avoided if, in addition to the inner barriers, doping atoms are also added to the outer layers of the superlattice, with an areal concentration of about half of the value used for the inner ones. In this work, we report the investigation of a superlattice sample with such a doping profile, grown by molecular beam epitaxy (MBE), by PL in high magnetic fields. Experiments showed that when the doping level is such that the miniband is fully populated, i.e. the Fermi level lies above the M_1 singularity, luminescence between Landau levels of the M_0 and M_1 valence and conduction band states can be detected. The miniband parameters can be obtained directly from the oscillations of the PL intensity as a function of the magnetic field, which is described by a doublet of frequencies. By measuring the oscillation frequencies as a function of the photon energy, we can estimate the miniband energy width, the

electron–hole pair reduced mass for in-plane movement, and the effective superlattice band gap. The superlattice band gap is lowered by the self-energy correction, arising from the electron exchange interaction, by an amount equal to the so-called *band gap renormalization* (BGR) [6]. For a superlattice with $1.42 \times 10^{12}\,\mathrm{cm}^{-2}$ electrons per period, our results show that the band gap is lowered by 23.4 meV. This value is intermediate between the BGR of 52 meV and 21 meV, estimated for a strictly two-dimensional or three-dimensional electron gas of equivalent density, respectively.

2. Experimental

The superlattice sample was grown by MBE and consisted of 20 GaAs quantum wells of 50 Å thickness, separated by 19 $Al_{0.21}Ga_{0.79}As$ inner barriers of thickness 50 Å. Low-angle x-ray reflectivity measurements confirmed the thickness of the layers. The internal AlGaAs barriers were delta-doped with Si at their centre, with an areal density of $1.9 \times 10^{12}\,\mathrm{cm}^{-2}$. The outer AlGaAs layers were delta-doped with half the same areal concentration, at a distance of 25 Å from the adjacent GaAs layer. Shubnikov–de Haas (SdH) measurements of in-plane conductivity were made on approximately square samples, with contacts in the corners, using currents of ∼200–400 μA. PL measurements were done in the Faraday geometry, using optical fibres and *in situ* miniature focusing optics. All measurements were done at 2 K.

3. Results and discussion

Figure 1 shows the Fourier transform of the SdH oscillations for the superlattice sample, for a magnetic field applied normal to the surface of the sample. Two peaks are observed, at $f_{\mathrm{SdH}}(M_1) = 23.4\,\mathrm{T}$ and $f_{\mathrm{SdH}}(M_0) = 34.9\,\mathrm{T}$. These peaks are associated with the 'belly' and 'neck' extremal orbits in the mini-Fermi surface [7], and can be labelled by the corresponding saddle points in the density of states, M_0 and M_1. To demonstrate this association, SdH measurements were done for a magnetic field direction tilted away from the normal to the surface of the sample. In tilted fields, the two peaks show the characteristic behaviour of quasi-three-dimensional electrons, whereby the M_0 and M_1 peaks cross over [8, 9], as shown in figure 2. According to Onsager's quasiclassical quantization formula, the Fourier frequencies in the SdH oscillations will be given by $f_{\mathrm{SdH}} = (\hbar/(2\pi e))\mathcal{A}_e$, where $\mathcal{A}_e$ are the extremal sections of the mini-Fermi surface, hence for a parabolic electronic in-plane dispersion we obtain

$$f_{\mathrm{SdH}}(M_0) = \frac{m_e \phi_e}{\hbar e}, \qquad f_{\mathrm{SdH}}(M_1) = \frac{m_e(\phi_e - \Delta_e)}{\hbar e}, \qquad (1)$$

where m_e is the electronic in-plane effective mass, ϕ_e the Fermi energy, and Δ_e the energy width of the miniband. The full and dashed lines shown in figure 2 are the theoretical M_0 and M_1 SdH frequencies, respectively, obtained from equation (1), by solving self-consistently the Schrödinger and Poisson equations, for an infinite $Al_{0.21}Ga_{0.79}As$/GaAs superlattice, with all GaAs and $Al_{0.21}Ga_{0.79}As$ layers being of width 50 Å, and doped in the middle of the internal barriers with $N_d = 1.42 \times 10^{12}\,\mathrm{cm}^{-2}$. The good agreement between theoretical and experimental Fourier frequencies demonstrates the presence of electrons confined by a superlattice potential, in close agreement with the design parameters.

The electronic effective mass, m_e, was estimated from the temperature dependence of the amplitude of the SdH oscillations, giving $m_e = 0.068 m_0$. Using the experimental values, $m_e = 0.068 m_0$, $f_{\mathrm{SdH}}(M_1) = 23.4\,\mathrm{T}$, and $f_{\mathrm{SdH}}(M_2) = 34.9\,\mathrm{T}$, equation (1) gives $\Delta_e = 19.6\,\mathrm{meV}$ and $\phi_e = 59.4\,\mathrm{meV}$.

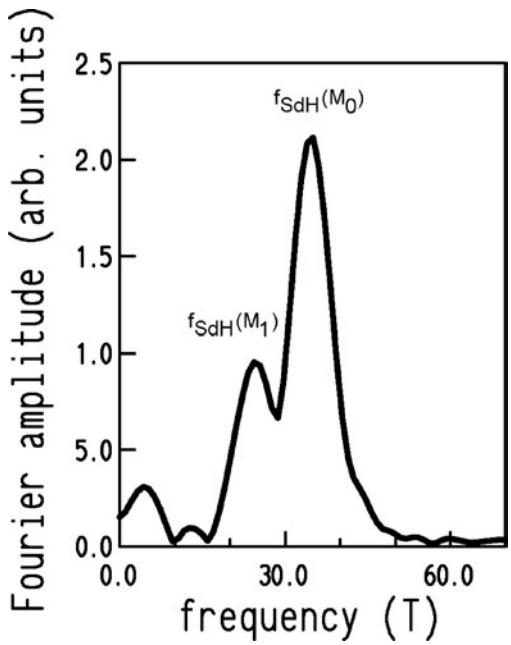

Figure 1. Fourier transform of the SdH oscillations for sample 2268, for a magnetic field applied normal to the surface of the sample. The labels indicate the saddle point in the density of states that originates a given frequency peak.

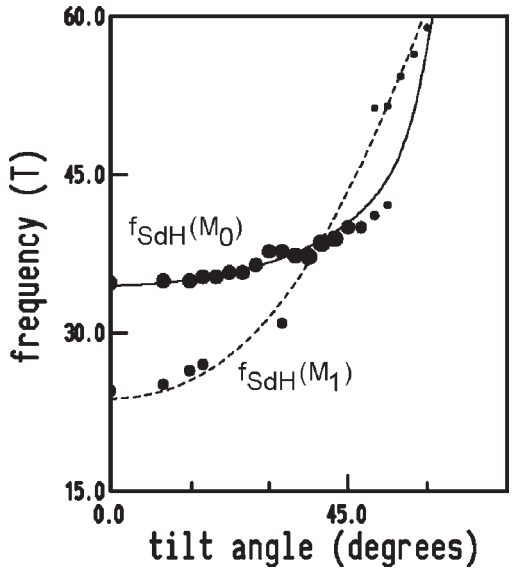

Figure 2. Peak position of the Fourier transform of the SdH oscillations as a function of the angle between the magnetic field direction and the normal to the surface of the sample. The area of each dot is proportional to the intensity of the peak. The full and dashed lines correspond to the theoretical frequencies for the oscillatory components associated with saddle points M_0 and M_1, respectively.

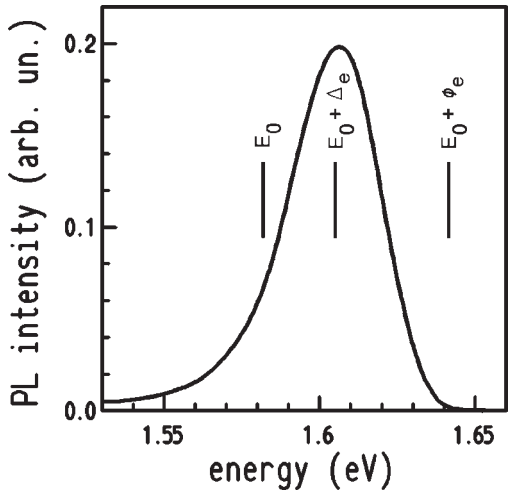

Figure 3. PL spectrum for the AlGaAs/GaAs superlattice. The superlattice band gap is indicated.

Figure 3 shows the PL spectrum at $T = 2\,\mathrm{K}$ for the superlattice. A broad emission band is seen above the GaAs gap, which is associated with recombinations between electrons and holes confined by the superlattice potential. The effective superlattice band gap, E_0, the energy corresponding to $E_0+\Delta_e$, and the energy corresponding to $E_0+\phi_e$, are shown in figure 3; these energies were estimated from the analysis below.

In order to demonstrate that the wide PL emission band shown in figure 3 arises from electron–hole recombinations by charge carriers confined by the superlattice potential, the PL spectra were studied as a function of the applied magnetic field. Figure 4 shows the PL intensity oscillations at fixed photon energies. The oscillations in the PL intensity, at a given photon energy $h\nu$, will be proportional to [10]

$$I(h\nu, B) \sim \sum_{N,N',k_e,k_h} |\langle\phi_h(N',k_h)|\phi_e(N,k_e)\rangle|^2 \times\delta\left[E_0+\left(N+\frac{1}{2}\right)\hbar\omega_e+E_e(k_e) +\left(N'+\frac{1}{2}\right)\hbar\omega_h+E_h(k_h)-h\nu\right], \tag{2}$$

where the summation is over electronic states, (N, k_e), that are situated below the Fermi level, and over hole states, (N', k_h), that contain photoexcited holes. Due to momentum conservation [11, 12], transitions occur only if $N' = N$ and $k_h = k_e = k$, and we obtain

$$I(h\nu, B) \sim |\langle\chi_h|\chi_e\rangle|^2 \sum_{N,k}\delta\left[E_0+\left(N+\frac{1}{2}\right)\frac{\hbar eB}{\mu} +E_e(k)+E_h(k)-h\nu\right], \tag{3}$$

where χ_e, χ_h are the electron and hole superlattice envelope wave functions, and μ is the reduced mass of the electron–hole pair. In the tight-binding approximation the electronic and hole miniband dispersion will be given by

$$E_e(k)=\frac{\Delta_e}{2}(1-\cos kd), \qquad E_h(k)=\frac{\Delta_h}{2}(1-\cos kd), \tag{4}$$

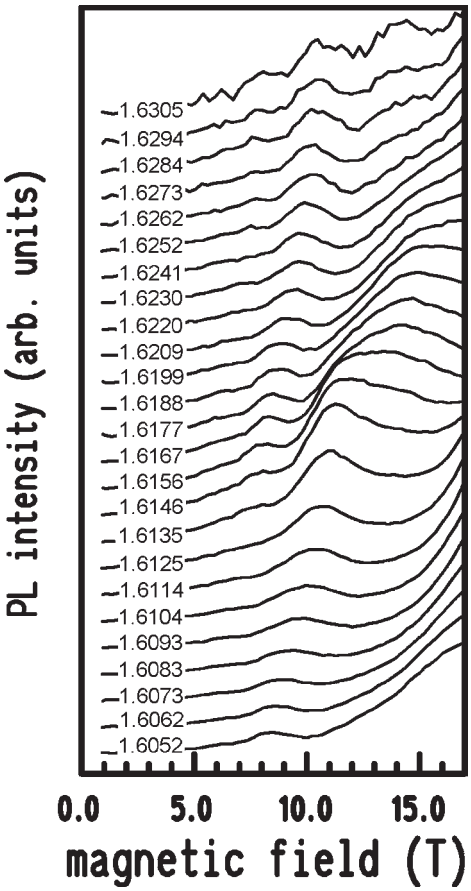

Figure 4. PL intensity oscillations at fixed photon energies. The photon energy corresponding to each curve is shown.

where d is the period of the superlattice, and by following the steps described in [13], from equations (3) and (4) we can obtain an analytical expression for the PL intensity oscillations:

$$I(h\nu, B) \sim -\exp\left(-\frac{2\pi\gamma\mu}{\hbar eB}\right) J_0\left(\pi\frac{\Delta_e+\Delta_h}{\hbar eB/\mu}\right) \times\cos\left(2\pi\frac{h\nu-E_0-((\Delta_e+\Delta_h)/2)}{\hbar eB/\mu}\right), \tag{5}$$

where γ is an energy level broadening parameter. Equation (5) yields a doublet of frequencies of oscillation, associated with the saddle points M_0 and M_1, whose values are

$$f_{\mathrm{PL}}(M_0)=\mu\frac{h\nu-E_0}{\hbar e}, \qquad f_{\mathrm{PL}}(M_1)=\mu\frac{h\nu-E_0-\Delta_e-\Delta_h}{\hbar e}. \tag{6}$$

Figure 5 shows the oscillations in the PL intensity as a function of the magnetic field for a photon energy of $h\nu = 1.6199\,\mathrm{eV}$, and a least-square fit to equation (5), including a monotonous parabolic background. The fit was obtained using the downhill simplex method [14]. To avoid falling into local minima, the minimization was done in two stages. In the first stage, $f_{\mathrm{PL}}(M_0)$ was fixed at the position of the main peak seen in the Fourier transform of the $I(B)$ oscillations, i.e. 22.3 T, while the value of the difference $(f_{\mathrm{PL}}(M_0) - f_{\mathrm{PL}}(M_1))$ was fixed at $(f_{\mathrm{SdH}}(M_0) - f_{\mathrm{SdH}}(M_1)) = 11.5\,\mathrm{T}$,

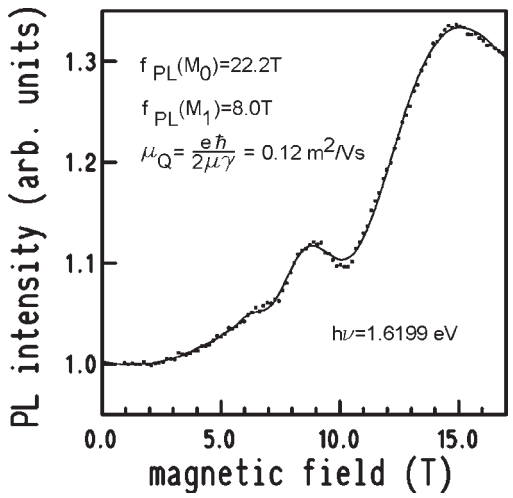

Figure 5. PL intensity oscillations at a photon energy of $h\nu = 1.6199$ eV. Dots are the experimental values and the full line is a fit with equation (5). The best fit values of the adjusting parameters are shown.

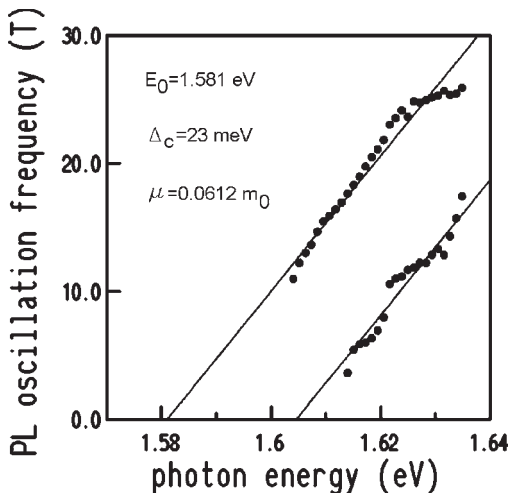

Figure 6. PL oscillation frequencies as a function of the photon energy.

and $\mu_Q = e\hbar/2\mu\gamma$ was fixed at $0.15\,\mathrm{m^2\,V^{-1}s^{-1}}$, which is the electronic quantum mobility estimated from the SdH measurements. The minimization at this stage produced preliminary values for the coefficients of the polynomial describing the non-oscillatory background, to be used as initial values in the second stage. In the second and final stage, all parameters were taken to be free. The fitting procedure yielded the values $f_{\mathrm{PL}}(M_0) = 22.2\,\mathrm{T}$ and $f_{\mathrm{PL}}(M_1) = 8.0\,\mathrm{T}$.

The fitting procedure was repeated for all photon energies measured. Figure 6 shows the frequencies of oscillations of the PL intensity in a magnetic field as a function of the photon energy. A linear dependence of the PL oscillation frequencies on the photon energy is obtained, in agreement with equation (6).

The straight lines depicted in figure 6 were obtained from a simultaneous linear fit of the two sets of data points with equation (6). The fit yields the intersection of the lines with the energy axis, which according to equation (6) will occur at the energies $h\nu = E_0 = 1.581\,\mathrm{eV}$ and $h\nu = E_0 + \Delta_e + \Delta_h = 1.604\,\mathrm{eV}$. The heavy-hole miniband energy width can be estimated theoretically from the solution of the Schrödinger–Poisson equations for the given structure, and we obtain $\Delta_h = 0.3\,\mathrm{meV}$, i.e. the hole dispersion can be ignored as a good approximation; hence, we can deduce $E_0 = 1.581\,\mathrm{eV}$ and $\Delta_e = 23\,\mathrm{meV}$. The latter parameter is in reasonable agreement with the electronic miniband width estimated from the SdH measurements, $\Delta_e = 19.6\,\mathrm{meV}$. The slope of the line determines the reduced effective mass of the electron–hole pair, i.e. $\mu = 0.0612m_0$. The estimated superlattice band gap, $E_0 = 1.581\,\mathrm{eV}$, can be compared to the theoretical value of the band gap, obtained from the $\boldsymbol{k}\cdot\boldsymbol{p}$ equation for this structure, $E_0^{\mathrm{th}} = 1.605\,\mathrm{eV}$, which does not take into account the lowering of the band gap due to many-body effects. By equating $E_0 = E_0^{\mathrm{th}} + \mathrm{BGR}$, we obtain $\mathrm{BGR} = -24\,\mathrm{meV}$. For an electron gas confined in two dimensions, the BGR is [15] $\mathrm{BGR}^{2\mathrm{D}} = -3.1(na_X^2)^{1/3}E_X$ [meV], where a_X and E_X are the exciton Bohr radius and binding energy, respectively, and $n = 1.42\times10^{12}\,\mathrm{cm^{-2}}$ is the areal density of electrons in the well. For a strictly two-dimensional electron gas, we substitute $E_X = 4R^*$, and an exciton radius of $a_X = a_B^*/2$, where R^* and a_B^* are the effective Rydberg and effective Bohr radius in bulk GaAs, respectively, to obtain $\mathrm{BGR}^{2\mathrm{D}} = -52\,\mathrm{meV}$. The finite thickness of the charges can be taken into account by calculating the exciton radius and binding energy for a 50 Å $\mathrm{GaAs/Al_{0.21}As_{0.79}As}$ quantum well, as described in [16, 17], to give $E_X = 10.34\,\mathrm{meV}$ and $a_X = 53$ Å, in which case $\mathrm{BGR}^{\mathrm{Q2D}} = -24\,\mathrm{meV}$. Finally, in the bulk, the BGR is given by [18] $\mathrm{BGR}^{3\mathrm{D}} = -3.5[n_{3\mathrm{D}}(a_B^*)^3]^{1/4}R^*$, where $n_{3\mathrm{D}} = n/d$ is the equivalent bulk carrier concentration, which gives $\mathrm{BGR}^{3\mathrm{D}} = -21.9\,\mathrm{meV}$. Thus, we find a BGR that is slightly larger than in the bulk, but is less than the BGR for a quasi-two-dimensional system.

In conclusion, superlattice structures of GaAs/AlGaAs composition were produced, with a modulation doping profile that prevents the formation of Tamm states. SdH measurements in tilted fields demonstrate the presence of electrons confined by a superlattice potential in close agreement with the design parameters. PL was studied in high magnetic fields, and a broad luminescence band was observed above the GaAs band gap. For a fixed photon energy within this broad PL band, the intensity of the luminescence oscillates as a function of the magnetic field applied perpendicular to the superlattice layers. The PL oscillations are described by a doublet of frequencies, which show a linear dependence on the energy of the photon, showing that it is due to recombinations of electron–hole pairs confined by the superlattice potential. We can estimate the superlattice parameters from the PL oscillations—the electronic miniband width Δ_e, the electron–hole pair reduced mass, μ, and the BGR, which we find is less than the BGR for a quantum well of the same barrier composition and well thickness, but greater than the BGR for a bulk GaAs degenerate electron gas.

Acknowledgments

This work was supported by FAPESP (Grant Nos 99/10359-7 and 01/00150-5) and CNPq (Grant No 306335/88-3).

References

[1] Helm M, Hilber W, Fromherz T, Peeters F M, Alavi K and Pathak R N 1993 *Phys. Rev.* B **48** 1601

[2] Grahn H T 1995 *Semiconductor Superlattices—Growth and Eletronic Properties* (Singapore: World Scientific)

[3] Yan R H, Simes R J, Ribot H, Coldren L A and Gossard A C 1989 *Appl. Phys. Lett.* **54** 1549

[4] Henriques A B, Oliveira R F, Souza P L and Yavich B 2001 *Physica* B **298** 320
Henriques A B 2001 *Appl. Phys. Lett.* **78** 691

[5] Steslicka M, Kucharczyk R, Akjouj A, Djafari-Rouhani B, Dobrzynski L and Davison S G 2002 *Surf. Sci. Rep.* **47** 93

[6] Schmitt-Rink S, Chemla D S and Miller D A B 1989 *Adv. Phys.* **38** 89

[7] Stormer H L, Eisenstein J P, Gossard A C, Wiegmann W and Baldwin K 1986 *Phys. Rev. Lett.* **56** 85

[8] Iye Y 1995 *Mater. Sci. Eng. B—Solid State Mater. Adv. Technol.* **31** 141

[9] Henriques A B, Hanamoto L K, Souza P L and Yavich B 2000 *Phys. Rev.* B **61** 13369

[10] Bastard G 1988 *Wave Mechanics Applied to Semiconductor Heterostructures* (Les Ulis: Les Editions de Physique)

[11] Roth L M, Lax B and Zwerdling S 1959 *Phys. Rev.* **114** 90

[12] Voisin P, Bastard G and Voos M 1984 *Phys. Rev.* B **29** 935

[13] Henriques A B 1994 *Phys. Rev.* B **50** 8658

[14] Nelder J A and Mead R 1965 *Comput. J.* **7** 308

[15] Schmitt-Rink S, Ell C, Koch S W, Schmidt H E and Haug H 1984 *Solid State Commun.* **52** 123

[16] Moore K J, Duggan G, Woodbridge K and Roberts C 1990 *Phys. Rev.* B **41** 1090

[17] Henriques A B 1992 *Superlatt. Microstruct.* **12** 527

[18] Reinecke T L and Ying S C 1979 *Phys. Rev. Lett.* **43** 1054